Bragg-type Brillouin spectroscopy of spin waves on ultrathin nickel nanowires

Yves Roussigné, Andrey Stashkevich,* and Salim-Mourad Chérif
Laboratoire des Sciences des Procédés et des Matériaux, CNRS-UPR 3407, Université Paris 13, 93430 Villetaneuse, France

Franck Vidal and Yunlin Zheng
Sorbonne Université, CNRS, Institut des NanoSciences de Paris, INSP, F-75005 Paris, France

Alexander Starkov
ITMO University, 49 Kronverksky pr., 197101 Saint Petersburg, Russia

(Received 24 July 2019; revised manuscript received 20 September 2019; published 4 October 2019)

We study the optical and magneto-optical properties of low-concentration arrays of ultrathin nickel nanowires by means of Brillouin spectroscopy of thermal magnons. Brillouin spectroscopy in such quasitransparent magneto-optical structures is dominated by the Bragg phase synchronism mechanism. At variance with ultrathin cobalt nanowire arrays, the Stokes/anti-Stokes scattering pattern is practically symmetrical. This feature is attributed to their peculiar optical properties.

DOI: 10.1103/PhysRevB.100.134406

I. INTRODUCTION

Self-assembled ferromagnetic nanowires embedded in a matrix are interesting both for applications (e.g., spin-torque nano-oscillators [1]) and for fundamental investigations (e.g., effective optical properties [2]). This interest is driven by an extremely broad range of creative ideas appearing in most important areas of human knowledge and technologies. Thus, rapid developments in the controlled movement of domain walls in magnetic nanowires by short pulses of spin-polarized current give promise of a nonvolatile memory device (such as the racetrack memory [3] comprised of an array of magnetic nanowires arranged horizontally or vertically on a silicon chip) with the high performance and reliability of conventional solid-state memory but at the low cost of conventional magnetic disk drive storage [4].

Of no less importance are periodic metallic structures in the area of metamaterials, artificially constructed media with enhanced and unique properties that are not seen in nature such as a negative index of refraction [5,6] or an epsilon near 0 [7]. These new materials are already finding applications in both existing and emerging technologies, such as in superlensing [6] and cloaking devices [8], optical microscopy [9], photonic circuits [10], hyperbolic polaritonic crystals [11], and plasmon-assisted nonlinear magneto-optics [12]. In order to achieve effects different from those naturally occurring in materials, functional inclusions, or meta-atoms, of subwavelength dimensions are used to manipulate incident electromagnetic radiation in the desired manner, and it is vital to have a direct means of probing and, hence, controlling the local state of polarization within such meta-atoms.

The most popular way of fabricating these systems is electrodeposition in a porous alumina matrix, being fast, inexpensive, and of high technological importance [13]. Another possibility is atomic layer deposition [14]. An alternative way is codeposition of the cylinders and the matrix taking advantage of the natural segregation and of the columnar growth. This technique allows for fabricating wires of much lower diameter than those obtained by other means [11,15–17].

Brillouin light scattering (BLS) is a well-established magneto-optical (MO) method that allows for probing spin waves (SWs) [18]. Most BLS experiments on magnetic materials are performed on opaque metallic media, typically thin films and multilayers [19], in which case the penetration depth of the light is reduced to a few tens of nanometers. In continuous thin films, the probed mode is propagating along the film surface. In this paper we study a very particular configuration, namely, assemblies of high and very thin nickel nanowires (height $\approx$ 400 nm, diameter $\approx$ 5 nm) embedded in a ceria matrix. Moreover, the concentration of the metallic inclusions in a perfectly transparent matrix is very low (not exceeding 4%). On the one hand, such a composite artificial material is characterized by low optical losses and thus light interacts with SW modes all along the nanowires. On the other hand, the dipolar interwire magnetic coupling is weak and dynamic magnetic behavior is represented by individual SW modes, localized on each wire and propagating along its length, i.e., normally to the surface of the composite film.

A low concentration of the metallic phase means that the effective optical parameters of the investigated composite medium are very close to those of the ceria matrix, which excludes any reliable information about what happens inside the metallic inclusions. At the same time, the BLS by magnons, which are localized exactly inside each Ni wire, provides a unique opportunity of probing the polarization state locally. Thus, our results suggest that the Brillouin spectroscopy, traditionally employed as a probe of magnon states, is an extremely sensitive technique for local probing photon states as

*stachkevitch@univ-paris13.fr

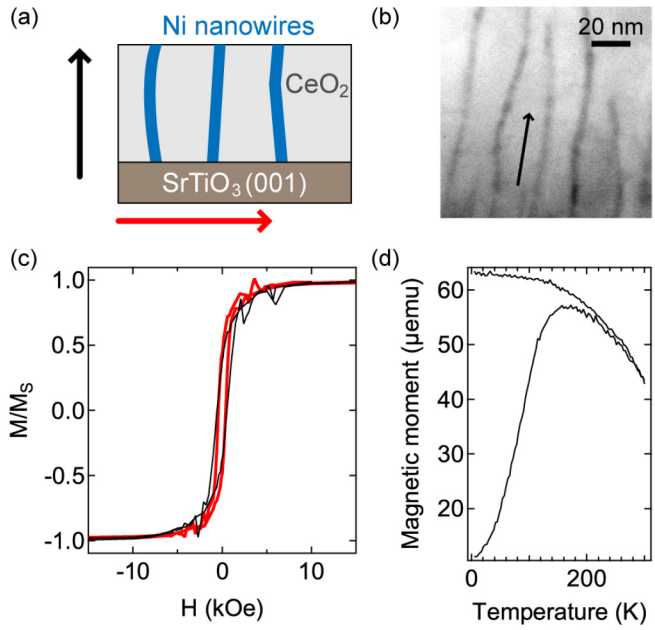

FIG. 1. (a) Sketch of the nickel nanowire assembly, (b) electron microscopy image of the nickel nanowire assembly, (c) in-plane (red curve) and out-of-plane (black curve) hysteresis loops obtained at $T = 100$ K, (d) field-cooling and zero-field-cooling measurements.

well, namely, for studying polarization-resolved local electric fields within nanoelements comprising an artificial material. More specifically, it has turned out that the effective optical properties of ultrathin Ni wires are very unusual, demonstrating a "quasidielectric" rather than a metallic behavior.

The latter can be attributed to a characteristic two-level structuring of the investigated composite medium; on the one hand (first level of structuring), the metallic constituent is realized in the form of ultrathin ($D = 4.3$ nm) and very long, with respect to the diameter ($t = 370$ nm), Ni wires. On the other hand (second level of structuring), each nanowire has a piecewise structure, being actually a stack of alternating 10-nm-high blocks with different magnetic and optical properties.

II. GROWTH AND MAGNETOSTATIC PROPERTIES OF THE NANOWIRE ASSEMBLY

A. Sample growth

The growth method used relies on sequential pulsed laser deposition (PLD) of Ni and CeO_2 under reductive conditions ($P_{growth} = 10^{-5}$ mb), leading to the self-assembly of Ni nanowires embedded in a $CeO_2/SrTiO_3(001)$ epilayer ($NiNW_{sto}$), as depicted schematically in Fig. 1(a). Thin films containing the nanowire assembly were grown on $SrTiO_3(001)$ (SurfaceNet GmbH) substrates using a quadrupled Nd:YAG laser (wavelength, 266 nm) operating at 10 Hz and a fluence in the 1–3 J · cm^{-2} range. NiO and CeO_2 targets were used. Prior to the growth of the nanowire assembly, a 4-nm-thick pure CeO_2 layer was deposited at 650°C and 10^{-2} mb of oxygen. This step ensures the subsequent epitaxial growth of the CeO_2 matrix under vacuum, with the following epitaxial relationship: $(001)_f/(001)_s$, $[110]_f//[100]_s$, $[1–10]_f//[010]_s$, where the s and f subscripts denote the substrate and film, respectively. After the buffer growth, the sample was kept at the same temperature and the pressure lowered to less than 10^{-5} mb. Growth of the self-assembled embedded wires was then carried out using sequential deposition of the compounds. Labeling n_{Ni} the number of laser shots on the NiO target and n_m the number of laser shots on the CeO_2 target, the growth was performed using a sequential process of the form $(n_{Ni} + n_m) \times N$, where N is the number of times the $(n_{Ni} + n_m)$ sequence is repeated. For samples grown in the framework of this study, we used $n_{Ni} = 10$, $n_m = 30$, and $N = 800$.

B. Structure

In the sample, metallic nanowire formation was evidenced using high-resolution and energy-filtered transmission electron microscopy data (acquired using a JEOL JEM 2100F equipped with a field-emission gun operated at 200 kV and a Gatan GIF spectrometer). The wires are mainly oriented perpendicular to the surface of the substrate and extend throughout the matrix thickness, t (for the sample studied, $t = 370$ nm). Nevertheless, many of them are not rectilinear [Fig. 1(b)]. The diameter, D, and density, d, of the wires were determined by collecting images in plane-view geometry. The results of such measurements are $D = 4.3 \pm 0.7$ nm and $d = (3.1 \pm 0.2) \times 10^{11}$ cm^{-2}.

A salient feature of this system is the small diameter of the wires, falling in the 4- to 5-nm range. Combined with their length, the aspect ratio should be large enough to ensure a pronounced magnetostatic anisotropy with an easy axis along the wire axis. The crystalline structure of the samples could also be determined using transmission electron microscopy and x-ray diffraction. In $NiNW_{sto}$, Ni is in cube-on-cube epitaxy with the CeO_2 matrix, as reported previously [17].

C. Magnetic properties

Static magnetic measurements were performed using a superconducting quantum device (SQUID) magnetometer (Quantum Design MPMS-5S). The data were corrected by removing the diamagnetic contribution of the substrate (obtained by extrapolating the high-field slope), in order to keep only the ferromagnetic contribution. Figure 1(c) shows the results of the magnetometry measurements with the magnetic field applied along the wire axis and perpendicular to it. The $NiNW_{sto}$ sample is nearly isotropic. Furthermore, it has a superparamagnetic behavior with a blocking temperature of 160 K as shown by field-cooling/zero-field-cooling measurements in Fig. 1(d).

This peculiar behavior is attributed to the magnetoelastic contribution to the anisotropy due to the Ni epitaxy with the CeO_2 matrix. Due to the lattice mismatch at the vertical heterointerface between the nanowires and the matrix, an axial tensile strain is present within the Ni nanowires. Such strain along the wire axis leads to a uniaxial magnetoelastic anisotropy that competes with the shape anisotropy [17]. As these two contributions tend to cancel each other and because the magnetocrystalline anisotropy of Ni is cubic, in-plane and out-of-plane magnetic cycles are nearly the same.

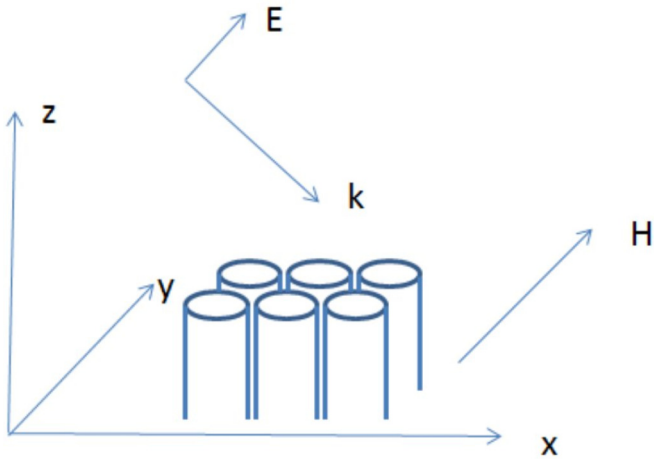

FIG. 2. Experimental arrangement: xy is the sample plane, the magnetic field H is applied along the y axis, and the incident light wave vector k lies in the zx plane as well as the optic electric field.

We close this section with some remarks on the impact of disorder in the system. As shown by TEM measurements, each wire can be regarded as a series of pieces with different local axis orientations. The disorientation from one piece to another reduces the coupling between pieces as well as the global shape anisotropy. It should also be noted that the Ni crystalline coherence length, deduced from the 002 peak in x-ray diffraction measurements, is 10 nm. This indicates that the wires can be regarded as a stack of short, 10-nm-high, cylinders having a finite aspect ratio of about 2 (a sort of nanoblock), potentially with a magnetoelastic anisotropy varying from piece to piece.

III. MAGNETO-OPTICAL SPIN-WAVE MEASUREMENTS

Magnetic oscillations have been probed using a laser beam (wavelength $\lambda_{\text{laser}} = 532$ nm) on the samples. Backscattered light has been analyzed with a tandem Fabry Perot interferometer (J. R. Sandercock). A magnetic field was applied in the plane of the sample (the in-plane geometry). The experimental arrangement is sketched in Fig. 2. The plane of incidence is perpendicular to the applied field. The polarization of the incident light is parallel to the plane of incidence (p polarization). The symmetry of the magneto-optical interactions is such that the polarization of the scattered wave is perpendicular to that in the incident wave, being along y (s polarization). The axes are chosen so that the z axis is parallel to the nanowires and the y axis is parallel to the applied field. In other words, the incident light electric field has two components, E_x and E_z, while that in the scattered wave has only one, E_y.

Let us begin with the analysis of the BLS spectral pattern, which, as it turns out, is very sensitive to the structure of the fields of interacting waves (optical as well as magnetic). More specifically, in this part we discuss the observed Stokes (S)/anti-Stokes (aS) asymmetry of the BLS spectral pattern. It should be stressed that there exists a fundamental difference between the classical BLS and the configuration explored in this paper. In conventional Brillouin spectroscopy, the principal aim is to trace the dispersion $f(q_{\text{SW}})$ of SW modes propagating in a continuous ferromagnetic film and characterized by an in-plane wave vector q_{SW}. It is extracted out of the measured BLS spectra, namely, from the Doppler frequency shift in the scattered light, in both the Stokes and the anti-Stokes line, as a function of the angle of incidence. Note that in BLS in the classical backscattering geometry

$$q_{\text{SW}} = q_{\text{in plane}} = 2\frac{2\pi}{\lambda_{\text{laser}}}\sin\varphi. \tag{1}$$

Here φ is the angle of incidence of the optical wave. In other words, conventionally, magneto-optical scattering by a magnon inverts only the *in-plane* component of the wave vector of the incident optical wave. The vertical component is inverted due to mirror reflection by an opaque metal film. Typically, optical and MO properties of metal films are supposed to be well known, which makes this task perfectly feasible.

In our particular case of a highly diluted sample the SW oscillations are localized on individual wires, since the dipole interactions between them are very weak and do not play any noticeable role in the dynamic magnetic behavior of the system. Consequently, the existence of collective Bloch-type modes propagating though the bulk of the composite film is excluded. In other words, one can regard the array of magnetic nanowires as an ensemble of individual independent SW oscillations localized along the axis of each wire. Their phases are absolutely uncorrelated. As a result, no in-plane dispersion features can be observed, in principle. BLS is a three-wave MO interaction and thus its efficiency depends on two major factors [20]: first, on the spatial correlation of the interacting waves

$$I_{\text{overlap}} = \iiint E^{(s)}(x,y,z)m(x,y,z)E^{(i)}(x,y,z)dV, \tag{2}$$

typically referred to as the overlap integral, and, second, on the "correlation" of their polarizations taking the form of their mixed product,

$$I_{\text{vec}} = (\vec{e}^{(s)}.(\vec{m}\times\vec{e}^{(i)})). \tag{3}$$

Here the functions $E^{(i)}(x,y,z)$, $E^{(s)}(x,y,z)$, and $m(x,y,z)$ describe the spatial distribution of the electric field in the incident and scattered optical waves and that of the magnetization in the scattering SW mode. Correspondingly, their polarizations are given by the unit vectors $\vec{e}^{(i)}$, $\vec{e}^{(s)}$, and $\vec{m}$.

Equations (2) and (3) are most helpful in understanding the mechanics of the MO interaction, especially in our particular case. More specifically, the first one [Eq. (2)] takes account of the rules of selectivity in the reciprocal space requiring phase synchronization of the waves taking part in the interaction, known as Bragg conditions. The second one [Eq. (3)] plays a similar role, specifying rules of the selection in the "space" of polarizations of the same waves, defined in the space of three-dimensional complex vectors. In the rest of this paper we refer to them as the spatial and vector factors, respectively. Since our composite medium is practically transparent, the Bragg spatial selectivity plays a major role in Brillouin scattering. In the backscattering configuration, $\vec{k}^{(i)} = -\vec{k}^{(s)}$, $\vec{q}_{\text{SW}} = -2\vec{k}^{(i)} = 2\vec{k}^{(s)}$, and, consequently,

$$2k = q_{\text{SW}}. \tag{4}$$

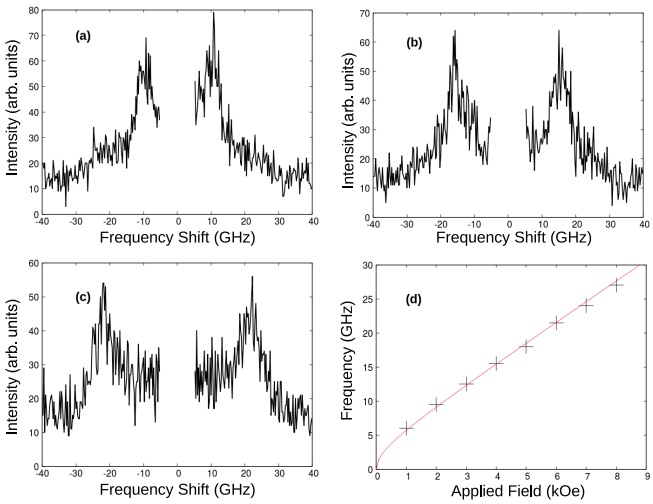

FIG. 3. Spectra obtained on assemblies of Ni nanowires for an in-plane applied field of (a) 2 kOe, (b) 4 kOe, and (c) 6 kOe. (d) Measured frequency versus applied field; the fitting curve corresponds to $\frac{\gamma}{2\pi}\sqrt{H(H+H_1)}$ with $\frac{\gamma}{2\pi} = 3$ GHz/kOe, $H_1 = 2.6$ kOe.

Here $\vec{k}^{(i)}$, $\vec{k}^{(s)}$ and $\vec{q}_{\mathrm{SW}}$ are the wave vectors of the incident optical wave, scattered optical wave, and a magnon propagating within the composite film. Strictly speaking, $k^{(s)}$ is not exactly equal to $k^{(i)}$ due to the Doppler frequency shift. However, since the SW frequency is at least four orders of magnitude lower than that of the optical wave, this difference is negligible and we may suppose that $k^{(s)} = k^{(i)} = k$. When this condition is satisfied the integrand no longer contains a rapidly oscillating function, which maximizes the overlap integral in Eq. (2). Here the term "magnon propagating within the composite film" needs to be clarified. There is a fundamental difference between the in-plane $q_{\text{in plane}}$ and the out-of-plane q wave-vector components. The latter can be regarded as a "genuine" wave vector corresponding to "vertical" (along z) SW modes localized on each wire (the Kittel mode in our case). Importantly, the state of polarization of such vertical magnons is its explicit function. At the same time, the former should rather be referred to as a "pseudo–wave vector." Since the phases of these vertical magnons are entirely independent from one another the distribution of the dynamic magnetization in the "xy" plane is "seen" by the incident optical wave as spatial white noise. Indeed, it is a random function with a correlation length equal to the interwire spacing, i.e., approximately 15 nm, which is small with respect to the optical wavelength. In other words, for an optical wave it is a δ-correlated random function. Naturally, it has no dispersion, and no polarization state can be attached to it (the latter is fully defined by q). The Fourier transform of a δ-correlated function is a constant that does not depend on $q_{\text{in plane}}$. In other words, the state of polarization of all "scattering" magnons, dictated by q, is the same for all angles of incidence, which is almost the same thing as $q_{\text{in plane}}$.

Typical spectra for different values of the saturating magnetic field are presented in Figs. 3(a)–3(c). The observed BLS spectral lines are much broader than expected, presumably because of disorientations of the pieces in the nanowires and the varying anisotropy revealed by the structural analysis. The mean frequency position of theses lines versus the applied field is plotted in Fig. 3(d) (crosses), while the solid line represents the results of theoretical modeling based on the dispersion of an SW mode on an individual SW mode whose effective wave number q is obtained from the Bragg condition (see above). As a matter of fact, our theoretical formalism is based on the approach presented in the classical paper by Arias and Mills [21]. The dynamic demagnetizing field is derived from a scalar potential; the Gauss equation for magnetism (no magnetic monopoles law) for this potential is solved together with the Landau-Lifshitz equation involving the dynamic demagnetizing field and the dynamic magnetization. The above-mentioned paper by Arias and Mills deals with axially magnetized nanowires, in which case a simultaneous exact solution of the Landau-Lifshitz equation together with the Gauss equation for magnetism is attainable. It is then possible to evaluate the dynamic stray field and thus estimate the dynamic dipolar coupling between nanowires. In the configuration of a perpendicularly magnetized nanowire, the symmetry of the problem is considerably reduced and an exact solution is no longer possible. Nevertheless, in the case of an individual ultrathin nanowire (diameter less than the exchange length), an exact solution can be found for the averaged dynamic magnetization across the nanowire section. From this solution, the dynamic stray field is calculated and thus the dynamic dipolar coupling is evaluated. Further details of these calculations can be found in Ref. [22].

Another source of broadening which is of purely magneto-optical origin and directly related to the length of nanowires is addressed later. To discuss the observed frequency variation, we first determine which modes are probed. As the incident light impinges on the sample at an angle of $\varphi = 20^\circ$ and as the matrix refractive index is $n_m = 2.2$, the refracted light direction makes an angle of only 9° with respect to the sample normal. Inside the matrix, the light propagates parallel to the wires. Following Ref. [22], the frequency of a propagating mode in a magnetic wire saturated in a direction perpendicular to its axis reads

$$f = \frac{\gamma}{2\pi}\sqrt{H_a H_b}, \tag{5}$$

with

$$H_a = \left(H - 2\pi M + \chi M + \frac{2A}{M}q^2 - \frac{2K}{M}\right)$$

and

$$H_b = \left(H - 2\pi M + \chi' M + \frac{2A}{M}q^2\right),$$

where A is the exchange constant, q is the wave number, and χ and χ' are dipolar factors which read $\chi = 4\pi/(1 - 2K_0'(qR)/(qRK_0(qR)))$ and $\chi' = 4\pi/(1 - qRK_1'(qR)/(K_1(qR)))$, where R is the wire radius, K_0 and K_1 are Bessel's functions, K_0' and K_1' are their first derivatives, and K is the perpendicular anisotropy. The large axial strain gives rise to a uniaxial magnetoelastic anisotropy that favors an easy plane. Using tabulated values of the magnetostriction coefficient [23], elastic constant of bulk Ni [24], and 0.7% axial strain gives $K = -6.8 \times 10^5$ erg/cm^3 for this contribution. Nevertheless, this anisotropy does not

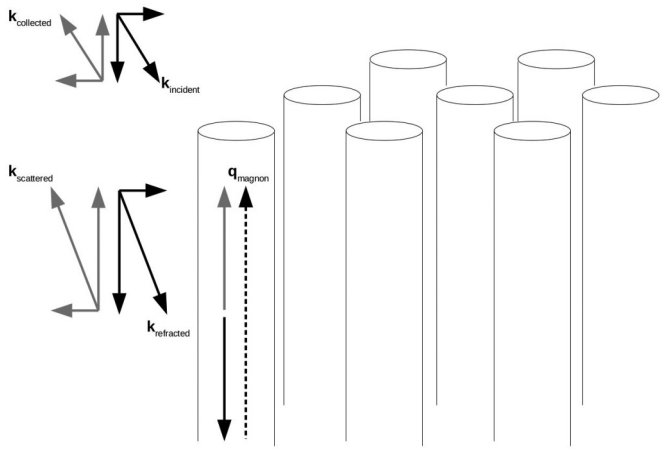

FIG. 4. Wave interaction.

completely cancel the shape anisotropy that favors an easy axis parallel to the wire, $\pi M^2 = 7.2 \times 10^5$ erg/cm^3. Assuming $A = 10^{-6}$ erg/cm, one can fit the experimental data with a wave number $q = 50$ rad/μm. The value of the SW wave number q corresponding to the Bragg condition $q_{\text{Bragg}} = 2.2 \times 4\pi/0.532$ rad/μm $= 52$ rad/μm, which is very close to the value extracted from magnetic measurements. The Bragg condition originating from the interaction between the optical wave whose wave number reads $-\sqrt{n_m^2 - \sin^2\varphi}\frac{2\pi}{\lambda_{\text{laser}}} \approx -2.2\frac{2\pi}{0.532}$ rad/μm and the magnetization propagating mode whose wave number is q. As the collected light is backscattered, its wave number is opposite to the incident one. This interaction is sketched in Fig. 4. Therefore $-\sqrt{n_m^2 - \sin^2\varphi}\frac{2\pi}{\lambda_{\text{laser}}} + q = \sqrt{n_m^2 - \sin^2\varphi}\frac{2\pi}{\lambda_{\text{laser}}}$, i.e., $q_{\text{Bragg}} = 2\sqrt{n_m^2 - \sin^2\varphi}\frac{2\pi}{\lambda_{\text{laser}}} \approx 2 \times 2.2\frac{2\pi}{0.532}$ rad/μm.

If the Bragg condition is not exactly satisfied, the interaction efficiency drops as $\text{sinc}((q - q_{\text{Bragg}})\frac{t}{2})$, where q_{Bragg} is the value, corresponding to the Bragg condition and q is a current value of the SW wave number. Here the argument $(q - q_{\text{Bragg}})\frac{t}{2}$ corresponds to the phase mismatch due to the deviation of q from its value imposed by the Bragg condition. This results in a corresponding broadening of the BLS spectral line. In our case the full width at half-maximum of the Bragg-condition-related line shape is about 5 GHz, which accounts for the unusually large value of the BLS line width in our experiments.

As one can see the Bragg condition of phase synchronism plays a very important role in transparent and semitransparent media, as in our case. Importantly, the Bragg condition is a universal principle that applies to all three-wave interactions, including magneto-optical, whatever the direction of the saturating magnetic field.

We now discuss the relative intensities of the Brillouin lines in the spectra. The Stokes line (negative frequency shift) and the anti-Stokes line (positive frequency shift) have close heights, which is not typical. Moreover, this is in stark contradiction with the results obtained in our previous paper on arrays of Co ultrathin nanowires; the measured spectra demonstrated a very pronounced Stokes/anti-Stokes asymmetry of unconventional type [25]. This was explained by a very peculiar state of optical polarization within each wire. Given the closeness of bulk optical constants of Ni and Co, one would expect a similarly pronounced asymmetry in the Ni BLS spectra, which is not, however, the case.

It should be noted that the effect of amplitude S/aS asymmetry is known for quite a long time, having been discovered as early as the late seventies [26]. Shortly afterwards, the subject was treated theoretically in full detail, first in the case of a semi-infinite ferromagnet [27], then in a finite-thickness ferromagnetic slab [28]. As a result, a most general formalism based on the fluctuation-dissipation theorem [29] and optical Green's functions for taking into account the optical properties of the structure has been developed. Thus both the thermal stochastic nature of the magnons and the macroscopic well defined magneto-optical properties of the structure were simultaneously taken into account. Later papers concentrated on the BLS cross section in thin films and multilayers [30,31].

At the early stage, the S/aS asymmetry was ascribed to the asymmetry of the spatial distribution of the surface Damon-Eshbach mode in two counter-propagating SWs: if in the first case it is localized near the top of the ferromagnetic film, in the second one its localization shifts to the bottom of the layer. This is perfectly justified for relatively thick structures. However, if the film thickness becomes comparable with the optical skin depth, another polarization-related mechanism becomes equally important. It was first pointed out in Ref. [32], dedicated to calculation of BLS backscattering intensities from pairs of exchange-coupled thin films in the Damon-Eshbach configuration. More particularly, it was shown that the ratio of the Stokes–to–anti-Stokes intensity is dependent upon the phase of the incident optical electric field in the magnetic films. This approach was convincingly applied to explain in simple terms the experimentally observed S/aS BLS intensity asymmetry of SW modes in ferromagnetic films and multilayers [33]. Importantly, during numerical estimations for a reference 17.1-nm-thick Fe single layer authors have tested the reliability of the simple and physically clear approximate technique with respect to the exact but cumbersome rigorous formalism. It has turned out that while major features can be explained successfully in terms of the approximate approach extra caution should be taken in interpreting the absolute numerical values. They can differ considerably, up to two times, from the exact ones.

For theoretical analysis of the optical properties, we use the general semiclassical theory of light scattering [34], which takes into account both the spatial correlation of the interacting fields in the form of an overlap integral, (2), and the "correlation" of polarizations of the interacting waves in the form of their mixed product, (3). Importantly, the integral, (2), contains the Bragg condition, which takes account of the rules of selectivity in the reciprocal space and whose role is preponderate in transparent and semitransparent media, as in our case. It is noteworthy that Eq. (3) is valid whatever the configuration of the magneto-optical interaction and the form of the ferromagnetic object. In certain configurations such as the dilute arrays of ultrathin nanowires considered in our paper an explicit analytical solution can be obtained for

both magnetic excitations and optical waves, which provides a simple physical picture of the mechanism of the interaction.

The description is further simplified by the fact that all the interacting fields are perfectly uniform. In the magnetic case it is due to the smallness of the wire diameter D with respect to the SW wavelength. It is due to the smallness of the wire diameter with respect to the skin depth in the optical case. Moreover, the diameter is also small with respect to the optical wavelength, which means that the optical field penetrates the nanosize sample according to the near-field diffraction pattern symmetrically from all sides, making the field inside a wire even more uniform. In more complicated situations, such as arrays of finite concentration of relatively wide nanorods of finite aspect ratio [35], a combined analyticonumerical approach is applied within which the functions describing field distributions are obtained numerically.

The first mechanism that can lead to a symmetric S/aS BLS pattern is linked to the superparamagnetic behavior of the structure under investigation with a blocking temperature of 160 K. At room temperature and without an external field the system is unblocked and the magnetization direction oscillates with a period much smaller than the time measurement, yielding no remnant magnetization. Thus, the symmetric S/aS pattern could be attributed to thermally excited periodic magnetization oscillations. Nevertheless, for a high applied field (e.g., $H = 6000$ Oe), this explanation does not work. Using a volume $V = \pi r^2 h$ with $r = 2.3$ nm and $h = 10$ nm (Ni lattice coherence length) and the Zeeman magnetic energy $HM = 6000 \times 500$ erg/cm^3, one obtains at room temperature $HMV/k_BT = 12$. The Langevin magnetization $M(\coth(\frac{HMV}{k_BT}) - \frac{k_BT}{HMV})$ is thus close to M even for such a small coherence length. This is confirmed by the magnetization loops; the sample is saturated by an external magnetic field of the order of several kOe.

Another explanation for the peculiar S/aS intensity ratio lies in the analysis of the particularities of the polarization states of the interacting waves. The degree of the S/aS asymmetry is monitored by a mixed product of polarizations of the three interacting waves: the incident optical wave, the scattered optical wave, and the scattering spin wave. Importantly, in this mixed product two polarizations are elliptical, namely, the incident p-type optical wave and the scattering SW mode, while the third one, the scattered s-type optical wave, is purely rectilinear. The difference between the Stokes and the anti-Stokes processes is the sign of the Doppler frequency shift; the anti-Stokes line is generated by a magnon with a positive frequency, while the Stokes line is due to scattering by a magnon with a negative frequency. The latter can be seen as time inversion for the scattering magnon, the direction of the magnetization precession being changed accordingly (anticlockwise for a positive magnon frequency and clockwise for a negative magnon frequency). This time reversal does not concern the p-type incident optical wave which retains its precession direction. Thus, physically we have two different configurations in MO three-wave mixing, two elliptical polarizations precessing in the same direction (anti-Stokes) and in opposite directions (Stokes). Mathematically, the time inversion in the magnon precession corresponds to complex conjugation and the above-mentioned mixed product is not invariant with respect to this complex conjugation.

The degree of ellipticity is described by the quantity P, which changes from 1 for right–circularly polarized fields to -1 for left–circularly polarized fields and it vanishes for linear polarization. Formally it is defined as

$$P = i((E'_x)^* E'_z - (E'_z)^* E'_x)/((E'_x)^* E'_x + (E'_z)^* E'_z). \quad (6)$$

If, for one reason or another, one of the elliptical polarizations turns rectilinear, the notion of the precession direction loses any sense and both configurations, Stokes and anti-Stokes, become equivalent, making the S/aS BLS pattern perfectly symmetric. This cannot be the ellipticity of magnon polarization; it is dominated by a purely circular shape imposed by the ferromagnetic resonance only slightly flattened due to the effect of dipolar interactions. In other words, it is fairly close to circular. All this leaves us with the only possible explanation of the observed symmetric S/aS spectra, i.e., the quasilinear polarization state of the otherwise elliptical incident p-type optical wave. The importance of the quantitative analysis of the spin-wave behavior of the sample, complementing the qualitative characterization outlined above, should not be underestimated either, especially since the reliability of Eq. (5) is convincingly confirmed by its adequate description of the experimental frequency dependence of the SW modes [see Fig. 3(d)]. The SW polarization is obtained from the Landau Lifshitz equation. According to Ref. [22], this equation reads $i\frac{\omega}{\gamma} m_x = -(H - 2\pi M + \chi M + \frac{2A}{M} q^2 - \frac{2K}{M}) m_z$, $i\frac{\omega}{\gamma} m_z = (H - 2\pi M + \chi' M + \frac{2A}{M} q^2) m_x$. Consequently $\frac{m_z}{m_x} = -i\frac{\omega}{\omega_1}$ with $\omega_1 = \gamma(H - 2\pi M + \chi M + \frac{2A}{M} q^2 - \frac{2K}{M})$ The symmetric BLS spectra can only be observed if the polarization of the incident p-type optical wave is close to rectilinear, which is not typically the case in bulk metals (see a detailed discussion of this issue in Ref. [19]). The scattered light intensity scales with $|E'_z m_x - E'_x m_z|^2 = |E'_z m_x|^2 |1 + i\frac{E'_x}{E'_z}\frac{\omega}{\omega_1}|^2$, where E'_x and E'_z are the components of the optical electric field inside the nanowire. Therefore the Stokes/anti-Stokes intensity ratio is

$$I_{\mathrm{St}}/I_{\mathrm{aSt}} = \left| \frac{1 - i\frac{E'_x}{E'_z}\frac{\omega}{\omega_1}}{1 + i\frac{E'_x}{E'_z}\frac{\omega}{\omega_1}} \right|^2. \quad (7)$$

The ratio $I_{\mathrm{St}}/I_{\mathrm{aSt}}$ is equal to 1 in the case of $\frac{E'_x}{E'_z} \in \mathbb{R}$. This in turn suggests lower values of the imaginary part of the effective dielectric permittivity. As the mean free path of the itinerant electrons that influence the optical properties is about 10 nm, they are scattered by the wire inhomogeneities. This may be related to the reduction of the imaginary part of the intrinsic permittivity.

In the case of Co nanowires studied previously by BLS [25], TEM measurements indicate that the nanowires are composed of oriented hexagonal grains with a length of the order of 30 nm, larger than the axial coherence length in Ni nanowires. Scattering effects are thus expected to be less pronounced in Co nanowires and the data could be modeled using the dielectric constant of bulk Co. It should be noted that a nonvanishing contribution to the optical constants stemming from enormous deformation within each Ni nanograin cannot be excluded.

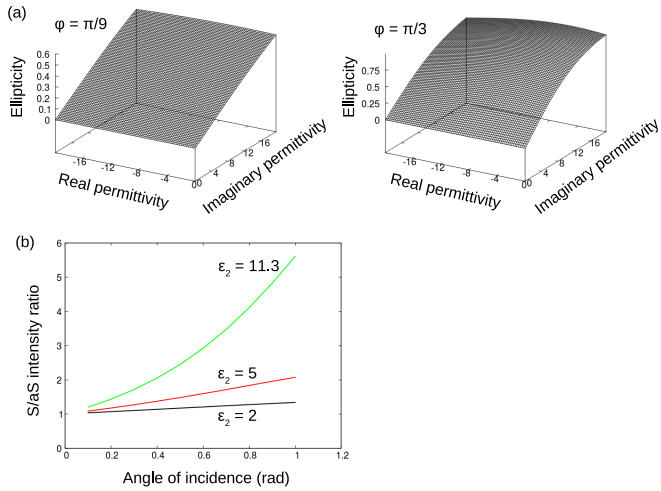

FIG. 5. (a) Ellipticity of the optical mode within a nanowire for $\varepsilon_m = 4.8$, $\varphi = \pi/9, \pi/3$, $H = 6$ kOe, $H_1 = 2.6$ kOe. (b) S/aS asymmetry as a function of the angle of incidence for several values of the imaginary part of the permittivity within a nanowire for $\varepsilon_m = 4.8$, $\varepsilon_1 = -6.9$, $\varepsilon_2 = 11.3,\ 5,\ 2$, $H = 6$ kOe, $H_1 = 2.6$ kOe.

To estimate the influence of the imaginary part of the effective dielectric permittivity ε_2 (with $\varepsilon_{Ni} = \varepsilon_1 + i\varepsilon_2$) on the S/aS asymmetry the following theoretical effort was undertaken. First, an analytical solution to the problem of refraction was found,

$$(E_x', E_z') \propto (2\varepsilon_m\sqrt{\varepsilon_m - \sin^2\varphi}, \sin\varphi(\varepsilon_{Ni} + \varepsilon_m)), \qquad (8)$$

where φ is the angle of incidence, which allowed expression of the ellipticity P of the optical mode within a nanowire as a function of the real and imaginary parts of epsilon.

Equation (8) is obtained in the following way. The incident light direction is $(\sin\varphi)\vec{u}_x - (\cos\varphi)\vec{u}_z$. Thus the light propagation direction in the matrix is $(\sin\varphi)\vec{u}_x - (\sqrt{\varepsilon_m - \sin^2\varphi})\vec{u}_z$. Therefore the light polarization is collinear to $(\sqrt{\varepsilon_m - \sin^2\varphi})\vec{u}_x + (\sin\varphi)\vec{u}_z$. In order to derive the light polarization in the wire, we use the relation between the interior field $\vec{E}'$ and the exterior field $\vec{E}$: $\varepsilon_m E_x' = \varepsilon_m E_x - 2\pi P_x$, where $4\pi P_x = (\varepsilon_{Ni} - \varepsilon_m)E_x'$ and $E_z' = E_z$. Consequently $E_x' = \frac{2\varepsilon_m}{\varepsilon_m + \varepsilon_{Ni}} E_x$ and $E_z' = E_z$.

The results of the numerical estimations are presented in Fig. 5(a), while Fig. 5(b) traces the S/aS asymmetry $I_{\mathrm{St}}/I_{\mathrm{aSt}}$ as a function of the angle of incidence for several values of ε_2. According to these calculations, if the imaginary part of the dielectric permittivity is decreased 2–3 times with respect to the conventional bulk values, the BLS spectra become sufficiently symmetric to coincide with the experimental data within the precision of the measurement technique; the raw spectra are rather noisy. Lower values of the imaginary part physically mean that the efficient composite medium becomes more transparent optically, which further justifies the relevance of the Bragg scattering mechanism. Interestingly, it is not the first time that thin nickel nanowires demonstrate very peculiar physical behavior. Indeed, the first publication on BLS from ferromagnetic nanowires [36] was based on 20-nm-thick Ni wire arrays obtained via conventional electrodeposition and featuring no pronounced inhomogeneity. However, to fit the experiment, the authors had to decrease the value of the exchange constant by 10 times.

In this paper we experimentally revealed an unexpectedly peculiar state of optical polarization in ultrathin nickel nanowires (4.3 nm wide), which can only be plausibly explained by a considerable reduction of the imaginary part of the dielectric permittivity of nickel at optical frequencies with respect to its conventional bulk value. We would like to stress that direct access to the optical and magneto-optical properties of metallic inclusions in a low-concentration structure like ours can only be provided via the unconventional Bragg-type Brillouin spectroscopy employed in this study. We stress that access to these properties is of great interest in order to optimize the elaboration of metamaterials. Finally, in the present system, the specific microscopic mechanisms explaining the reduction of the imaginary part of the dielectric constant are yet to be identified. This should stimulate further efforts in order to explain the response of nanoscale metallic systems of potential interest in the fields of spintronics, nano-optics, and metamaterials.

IV. CONCLUSION

This study deals with magnetic Ni nanowires embedded in a $CeO_2/SrTiO_3(001)$ transparent matrix grown by pulsed laser deposition. The Ni nanowires have a small diameter (4.3 ± 0.7 nm) and are not perfectly oriented as shown by transmission electron microscopy images. Due to competition between the magnetoelastic anisotropy induced by the Ni epitaxy in CeO_2 and the shape anisotropy, the system exhibits a quasi-isotropic behavior and has a low blocking temperature (around 160 K). The magnetization oscillations in nanowires have been investigated by Brillouin light spectroscopy. It was shown that in quasitransparent samples the conventional conservation of the in-plane component of the wave vector is replaced with the Bragg condition. The measured frequency corresponds to the magnetization wave propagating along the nanowires with a wave number deduced from the Bragg condition. Moreover, this purely optical mechanism contributes significantly to the broadening of the BLS spectral lines. At variance with previously studied Co nanowire arrays, the Stokes and anti-Stokes lines in BLS spectra measured for Ni nanowire arrays are characterized by an untypically symmetrical intensity pattern. This can be explained by quasirectilinear polarization of the optic wave inside the nanowires. Mathematically the latter results from the reduction of the imaginary part of the nickel permittivity possibly related to scattering of itinerant electrons by the inhomogeneities in the crystal structure.

ACKNOWLEDGMENTS

The authors thank D. Demaille for TEM measurements, J.-M. Guigner (IMPMC) for access to the TEM facilities, and the staff of the MPBT platform of Sorbonne Université for their assistance.

[1] F. Abreu Araujo, L. Piraux, V. A. Antohe, V. Cros, and L. Gence, Appl. Phys. Lett. **102**, 222402 (2013).

[2] C. R. Simovski, P. A. Belov, A. V. Atrashchenko, and Y. S. Kivshar, Adv. Mater. **24**, 4229 (2012).

[3] S. S. P. Parkin, M. Hayashi, and T. L., Science **320**, 190 (2008).

[4] R. Lavrijsen, J. H. Lee, A. Fernandez-Pacheco, D. C. M. C. Petit, D. Mansell, and R. P. Cowburn, Nat. Lett. **493**, 647 (2013).

[5] D. R. Smith, W. J. Padilla, D. C. Vier, S. C. Nemat-Nasser, and S. Schultz, Phys. Rev. Lett. **84**, 4184 (2000).

[6] J. B. Pendry, Phys. Rev. Lett. **85**, 3966 (2000).

[7] R. J. Pollard, A. Murphy, W. R. Hendren, P. R. Evans, R. Atkinson, G. A. Wurtz, A. V. Zayats, and V. A. Podolskiy, Phys. Rev. Lett. **102**, 127405 (2009).

[8] D. Pendry, J. B. Schurig, and D. R. Smith, Science **312**, 1780 (2006).

[9] A. Alu and N. Engheta, Phys. Rev. Lett. **105**, 263906 (2010).

[10] N. Engheta, Science **317**, 1698 (2007).

[11] W. Dickson, S. Beckett, C. Mc Clatchney, A. Murphy, D. O'Connor, G. A. Wurtz, R. Pollard, and A. V. Zayats, Adv. Mater. **27**, 5974 (2015).

[12] V. L. Krutyanskiy, I. A. Kolmychek, E. A. Gan'shina, T. V. Murzina, P. Evans, R. Pollard, A. A. Stashkevich, G. A. Wurtz, and A. V. Zayats, Phys. Rev. B **87**, 035116 (2013).

[13] U. Ebels, J. L. Duvail, P. E. Wigen, L. Piraux, L. D. Buda, and K. Ounadjela, Phys. Rev. B **64**, 144421 (2001).

[14] D. Cola, M. Darques, O. Fruchart, and L. Cagnon, Appl. Phys. Lett. **98**, 112501 (2011).

[15] F. Vidal, Y. Zheng, J. Milano, D. Demaille, P. Schio, E. Fonda, and B. Vodungo, Appl. Phys. Lett. **95**, 152510 (2009).

[16] P. Schio, F. Vidal, Y. Zheng, J. Milano, E. Fonda, D. Demaille, B. Vodungbo, J. Varalda, A. J. A. de Oliveira, and V. H. Etgens, Phys. Rev. B **82**, 094436 (2010).

[17] F. J. Bonilla, A. Novikova, F. Vidal, Y. Zheng, E. Fonda, D. Demaille, V. Schuller, A. Coati, A. Vlad, Y. Garreau, M. Sauvage-Simkin, Y. Dumont, S. Hidki, and V. H. Etgens, ACS Nano **7**, 4022 (2013).

[18] M. Cottam and D. Lockwood, *Light Scattering in Magnetic Solids* (Wiley-Interscience, New York, 1986).

[19] P. Grünberg, Light scattering from spin-waves in thin films and layered magnetic structures, in *Light Scattering in Solids V*, edited by M. Cardona and G. Güntherodt, Topics in Applied Physics Vol. 66/1 (Springer, Berlin, Heidelberg, 1989).

[20] A. Stashkevich, Light scattering from spin-waves in thin films and layered magnetic structures, in *High-Frequency Processes in Magnetic Materials*, edited by A. N. Slavin and G. Srinivasan (World Scientific, Singapore, 1995).

[21] R. Arias and D. L. Mills, Phys. Rev. B **63**, 134439 (2001).

[22] Y. Roussigné, S. M. Chérif, A. A. Stashkevich, F. Vidal, and Y. Zheng, J. Appl. Phys. **118**, 233903 (2015).

[23] S. Kadowaki and M. Takahashi, J. Phys. Soc. Jpn. **50**, 1154 (1981).

[24] H. J. Leamy and H. Warlimont, Phys. Status Solidi (b) **37**, 523 (1970).

[25] A. A. Stashkevich, Y. Roussigné, A. N. Poddubny, S.-M. Chérif, Y. Zheng, F. Vidal, I. V. Yagupov, A. P. Slobozhanyuk, P. A. Belov, and Y. S. Kivshar, Phys. Rev. B. **92**, 214436 (2015).

[26] P. Grünberg and F. Metawe, Phys. Rev. Lett. **39**, 1561 (1977).

[27] R. E. Camley and D. L. Mills, Phys. Rev. B **18**, 4821 (1978).

[28] M. Cottam, J. Phys. C **12**, 1709 (1979).

[29] D. Chandler, *Introduction to Modern Statistical Mechanics* (Oxford University Press, New York, 1987).

[30] M. Cottam, J. Phys. C: Solid State Phys. **16**, 1573 (1983).

[31] Y. Roussigné, F. Ganot, C. Dugautier, P. Moch, and D. Renard, Phys. Rev. B **52**, 350 (1995).

[32] J. F. Cochran and J. R. Dutcher, J. Appl. Phys. **64**, 6092 (1988).

[33] R. Zivieri, P. Vavassori, L. Giovannini, F. Nizzoli, E. E. Fullerton, M. Grimsditch, and V. Metlushko, Phys. Rev. B **65**, 165406 (2002).

[34] G. B. Benedek and K. Fritsch, Phys. Rev. **149**, 647 (1966).

[35] A. A. Stashkevich, Y. Roussigné, P. Djemia, S. M. Chérif, P. R. Evans, A. P. Murphy, W. R. Hendren, R. Atkinson, R. J. Pollard, A. V. Zayats, G. Chaboussant, and F. Ott, Phys. Rev. B **80**, 144406 (2009).

[36] Z. K. Wang, M. H. Kuok, S. C. Ng, D. J. Lockwood, M. G. Cottam, K. Nielsch, R. B. Wehrspohn, and U. Gösele, Phys. Rev. Lett. **89**, 027201 (2002).